Measurement Report: Hygroscopicity and mixing state of submicron aerosols in the lower free troposphere over central China: local, regional and long-range transport influences

Jingnan Shi[1,★], Zhisheng Zhang[2,★], Li Li[3], Li Liu[4,#], Yaqing Zhou[5,6], Shuang Han[7], Shaobin Zhang[5,6], Minghua Liang[5,6], Linhong Xie[5,6], Weikang Ran[3], Shaowen Zhu[5,6], Hanbing Xu[8], Jiangchuan Tao[5,6], Alfred Wiedensohler[9], Qiaoqiao Wang[5,6], Qiyuan Wang[3], Nan Ma[5,6], Juan Hong[5,6,#]

[1]Institute of Facility Agriculture of Guangdong Academy of Agricultural Sciences, Guangzhou, 510640, China
[2]Guangdong Provincial Key Laboratory of Water and Air Pollution Control, South China Institute of Environmental Science, Ministry of Ecology and Environment, Guangzhou, 510655, China
[3]State Key Laboratory of Loess and Quaternary Geology, Key Lab of Aerosol Chemistry and Physics, Institute of Earth Environment, Chinese Academy of Sciences, Xi'an, 710061, China
[4]Guangzhou Institute of Tropical and Marine Meteorology of China Meteorological Administration, GBA Academy of Meteorological Research, Guangzhou, 510640, China
[5]Institute for Environmental and Climate Research, Jinan University, Guangzhou, 511443, China
[6]Guangdong-Hongkong-Macau Joint Laboratory of Collaborative Innovation for Environmental Quality, Guangzhou, 511443, China
[7]Department of Geography, College of Science, Qiqihar University, Qiqihar 161006, China
[8]School of Computer Science and Engineering, Sun Yat-Sen University, Guangzhou, 510006, China
[9]Institute for Tropospheric Research, Permoserstr. 15, Leipzig, 04318, Germany
★These authors contributed equally to this work.

Correspondence to: Juan Hong (juanhong0108@jnu.edu.cn) and Li Liu (liul@gd121.cn)

Abstract.

Understanding the hygroscopicity and mixing state of atmospheric aerosol particles is crucial for accurately assessing their role in cloud formation and subsequent climate impacts. However, measurements in the lower free troposphere - a representative atmospheric layer characterizing regional background conditions in aerosol transport and atmospheric evolution - remain sparse, especially in regions influenced by both anthropogenic emissions and long-range transported air masses. This study adds further data on size-resolved hygroscopicity and mixing state measurements of aerosols at Mt. Hua (2060 m a.s.l., central China) during October-November 2021 using a Hygroscopicity Tandem

Formatted: Highlight

Deleted: Understanding the hygroscopicity and mixing state of atmospheric aerosol particles is crucial for

Deleted: improving predictions of cloud formation and climate impacts.

Differential Mobility Analyzer (HTDMA). Results reveal a clear size-dependence of aerosol hygroscopicity, with the mean hygroscopicity parameter (κ_{mean}) increased from 0.20 for 30 nm particles to 0.30 for 200 nm particles. The ambient submicron aerosols were primarily externally mixed, dominated by more-hygroscopic (MH) particles, with no significant diurnal variation, indicating minimal influence from boundary layer dynamics. Starting from November 6, the combined influence of mineral dust and regional heating activities led to a notable reduction in aerosol hygroscopicity, especially in larger particles. This decline was driven by an increase in weakly hygroscopic components such as mineral dust, black carbon, and organic compounds, highlighting the impact of both long-range transport and regional emissions on aerosol composition. Notably, during episodes of striking high relative humidity (RH > 80%) in Cluster 5, atmospheric aerosols containing mineral dust showed unexpected hygroscopic enhancement, suggesting in situ RH-driven chemical processing that increased aerosol hygroscopicity. Atmospheric aerosols at Mt. Hua displayed distinct hygroscopic properties compared to other high-altitude sites, underscoring regional differences in aerosol sources and free tropospheric processing. These findings advance our understanding of aerosol aging and processes in the lower free troposphere over central China, and offer crucial observational constraints for modeling aerosol–cloud interaction and regional climate impacts.

Formatted: Highlight

Deleted:

Formatted: Font: Italic, Highlight

Formatted: Subscript, Highlight

Formatted: Highlight

Deleted: Results demonstrate size-dependent hygroscopicity, with the mean hygroscopicity parameter (κ_{mean}) increasing from 0.20 (30 nm) to 0.30 (200 nm).

Formatted: Highlight

Deleted: aerosols in Cluster 5 showed enhanced hygroscopicity under high relative humidity (RH > 80 %), likely due to multi-phase or aqueous-phase reactions that altered their chemical composition. Aerosols originating from Mongolia deserts tended to be less hygroscopic, associated with an enhanced number fraction of less-hygroscopic (LH) mode particles relative to those from other sources. However,

Formatted: Highlight

Formatted: Font: 10 pt, Bold

1 Introduction

Aerosol hygroscopicity, defined as the ability of aerosol particles to absorb water vapor from the surrounding atmosphere (Cai et al., 2017; Petters and Kreidenweis, 2007; Swietlicki et al., 2008), is a critical property that influences Earth's radiative balance by altering particle size distributions and associated optical properties (Bai et al., 2018; Cheng et al., 2008; Hong et al., 2018; Su et al., 2010). This property also plays a pivotal role in cloud processes by modulating the concentration of cloud condensation nuclei (CCNs) and affecting the lifetime and microphysical properties of clouds, thereby exerting indirect effects on regional and global climate (Liu et al., 2013; Rosenfeld et al., 2014). Additionally, aerosol hygroscopicity can regulate heterogeneous and multiphase chemistry through promoting the uptake reaction rates of different trace gases (e.g., SO_2, NO_X) within hydrated aerosols with elevated aerosol liquid water content (Tong et al., 2020; Wang et al., 2020; Wu et al., 2018b). Beyond atmospheric impacts, it also governs respiratory health by determining the deposition efficiency and site

of inhaled particles within the human respiratory tract (Farkas et al., 2022).

High-altitude alpine regions in the free troposphere, distanced from local pollution yet strongly influenced by long-range transport, serve as representative of the atmospheric characteristics on a large-scale (Colbeck et al., 1998). Additionally, these regions can also signify the interactions between the free troposphere and the planetary boundary layer (PBL) through vertical advection of lowland pollutants during the diurnal PBL evolution (Holmgren et al., 2014). Despite these significance, comprehensive measurements of aerosol hygroscopicity in such high-altitude environments still remain scarce, with only very few studies available to date. For instance, observations at Jungfraujoch, Switzerland (3580 m a.s.l.), revealed that injections of PBL air reduced the hygroscopicity of the background free-tropospheric aerosols (Kammermann et al., 2010). Similarly, aerosols measured at the Monte Cimone Observatory in Italy (2165 m a.s.l.) showed similar hygroscopicity compared to Jungfraujoch aerosols, though occasionally influenced by the long-range-transported African dust (Dingenen et al., 2005). At the slightly lower-altitude Puy de Dôme station (1465 m a.s.l.), aerosols displayed intermediate hygroscopicity due to mixed influences from oceanic, continental, African and local air masses (Holmgren et al., 2014).

However, these limited observations have been largely confined to European alpine sites, leaving a critical gap in understanding aerosol hygroscopicity in other high-altitude regions, particularly in Asia, where atmospheric conditions and pollution sources differ substantially. Mt. Hua (2060 m a.s.l.), located in central China, presents an ideal setting for such investigations due to its unique geographic position. The mountain lies adjacent to the heavily polluted Guanzhong Basin, which experiences intense anthropogenic emissions, while also being downwind of the vast Mongolian deserts. This particular exposure makes the site susceptible to both regional pollution plumes and frequent dust intrusions, most likely resulting in a more complex particle composition compared to typical ground-level measurements. It has been documented that (Wang et al., 2012) mineral dust levels in aerosols at Mt. Hua increased sharply during dust storms originated from the Mongolian deserts. Notably, this mineral dust can undergo chemical modification after transport through polluted regions, interacting with other anthropogenic pollutants. Such processes may further complicate the aerosol composition that ultimately reached Mt. Hua and consequently alter the hygroscopic properties of particles at the site. However, the combined influence of these mixed sources on aerosol hygroscopicity at Mt. Hua has yet to be systematically evaluated.

In this study, we present the first direct measurements of aerosol hygroscopicity and mixing state at the summit (~2060 m a.s.l.) of Mt. Hua during early winter of 2021, using a self-assembled Hygroscopicity Tandem Differential Mobility Analyzer (HTDMA). To our knowledge, this work provides the first comprehensive investigation of aerosol hygroscopicity at a high-altitude site in central China. By analyzing the effects of diurnal cycles and air mass types on aerosol hygroscopicity, we gain new insights into the atmospheric processing and regional evolution of background aerosols.

2 Site and measurement methods

2.1 Site description

The field campaign was conducted at the summit of Mt. Hua (34°28′N, 110°05′E; 2060 m a.s.l), located in the central part of the Guanzhong Basin of western China, from October 15 to November 19, 2021. The sampling area was predominantly covered with vegetation and was distant from anthropogenic influence, with the nearest city (Huayin) being about 5.9 kilometers away from the mountain base. Being mostly situated within the free troposphere as suggested earlier (Shen et al., 2023), this site effectively represent the free tropospheric background atmospheric conditions in this region.

2.2 Aerosol hygroscopicity measurements and data analysis

A self-assembled HTDMA system was used to characterize aerosol hygroscopicity during this study. A detailed description and the working principles of the HTDMA system can be found in previous studies (Han et al., 2022; Tan et al., 2013). Specifically, the hygroscopic growth factor (GF) was measured for particles with dry diameter of 30, 60, 100, 150 and 200 nm at 90 % relative humidity (RH). The system was calibrated once a week using ammonium sulfate, which is a reference material with well-characterized hygroscopic properties.

In this study, the hygroscopicity parameter, κ, introduced by Petters and Kreidenweis as (Petters and Kreidenweis, 2007), was used to describe the hygroscopicity properties of aerosol particles based on the measured GF as :

$$\kappa = (GF^3 - 1)\left(1 - \frac{RH}{K_e}\right), \quad (1)$$

$$K_e = \exp\left(\frac{4\sigma_{s/a}M_w}{RT\rho_w D_{dry}}\right), \quad (2)$$

Deleted: exp$ADdryGF$
Deleted: RH
Deleted: -1
Formatted: Highlight
Formatted: Highlight
Formatted: Highlight
Formatted: Highlight
Formatted: Highlight
Formatted: Highlight
Formatted: Highlight
Formatted: Highlight
Formatted: Highlight
Formatted: Highlight
Formatted: Highlight
Deleted: A
Deleted: $=$
Deleted: $\frac{4\sigma_{s/a}M_w}{RT\rho_w}$
Deleted:
Deleted:
Formatted: Highlight
Formatted: Highlight
Formatted: Highlight
Formatted: Highlight
Formatted: Highlight
Formatted: Highlight
Formatted: Highlight
Formatted: Highlight
Formatted: Highlight
Formatted: Highlight
Formatted: Highlight
Formatted: Highlight
Formatted: Highlight

GF is the hygroscopic growth factor measured by HTDMA at 90 % RH. D_{dry} is defined as the particle diameter selected by the first DMA under dry conditions (RH < 10 %) at 25 °C. ρ_w and Mw are the density and molecular weight of water. $\sigma_{s/a}$ is the surface tension of the droplets, which is assumed to be that of pure water ($\sigma_{s/a}$ = 0.0728N m^{-2}). R is the ideal gas constant and T is the ambient temperature. K_{ka} is the Kelvin correction factor term. The κ probability density function (κ-PDF), indicative of a statistical distribution that describes the variation in hygroscopicity among an aerosol population, was derived from the GF probability density function (GF-PDF), which was retrieved from the measured GF distribution function (GF-MDF) using the TDMAinv algorithm (Gysel et al., 2009).

Given the complex mixing states of ambient aerosols, aerosols are commonly classified into distinct hygroscopic groups based on the hygroscopicity parameter κ (Liu et al., 2011), as more-hygroscopic aerosols normally have larger κ values and less-hygroscopic particles have smaller ones. In the present work, two different hygroscopic modes were clearly identified. Accordingly, aerosol particles were categorized into two modes with respect to their hygroscopicity: a less-hygroscopic mode (LH, κ <= 0.2) and a more-hygroscopic mode (MH, κ > 0.2), consistent with the approach of Shi et al. (2022). The values of κ for each mode were calculated as the volume-equivalent mean derived from the κ-PDF within the respective κ boundaries.

Formatted: Font colour: Auto, Highlight
Formatted: Font: Not Italic, Font colour: Auto, Highlight
Formatted: Indent: First line: 0 ch
Deleted: D_{dry} is the size of the particles.
Deleted:
Formatted: Highlight
Formatted: Font colour: Auto
Formatted: Font colour: Auto, Subscript
Formatted: Font colour: Auto
Deleted: .
Due to the complex mixing states of ambient aerosol, …
Formatted: Font colour: Auto
Formatted: Font colour: Auto
Formatted: Font colour: Auto

Deleted: we divided aerosol particles into two modes with respect to their hygroscopicity: a less-hygroscopic mode (LH, κ <= 0.2) and a more-hygroscopic mode (MH, κ > 0.2) (Shi et al., 2022).

2.3 Other measurements

In this study, the particle number size distribution (8-750 nm) was measured using a Scanning Mobility Particle Sizer (SMPS, Model 3080, TSI Inc., USA). Water-soluble inorganic ions (Na^+, NH_4^+, NO_3^-, SO_4^{2-}) were quantified by an online ion chromatograph (online measurement-9000, Thermo Fisher Scientific, USA) through a $PM_{2.5}$ sharp-cut cyclone inlet, while the mass concentration of elemental carbon (EC) and organic carbon (OC) were determined using an OC/EC aerosol analyzer (Sunset Laboratory, Forest Grove, OR) (Bae et al., 2004).

In addition to online measurements of the particle chemical composition, offline samples were collected twice daily (07:00–19:00 and 19:00–07:00 the following day) on quartz fiber filters using a high-volume air sampler (TISCH, TE6070DV-BL) operating at a flow rate of 1.13 m^3·min^{-1}. All collected samples were wrapped in foil and stored at ~ 4 °C until analysis. Field blank samples were also collected

Deleted: a
Deleted: URG
Deleted: Ambient Ion Monitor (
Formatted: Highlight
Deleted: Thermo Fisher

before and after the sampling by mounting a prebaked blank filter onto the sampler for about 10 min without sucking any air. The major chemical components of $PM_{2.5}$, including major and trace elements as well as water-soluble ions, were subsequently analyzed using an energy-dispersive X-ray fluorescence spectrometer (ED-XRF, Epsilon 4, Malvern Panalytical, Netherlands) and ion chromatography (940 Professional IC Vario, Metrohm). Detailed information for the offline chemical analysis can be found in (Feng et al., 2023).

Meteorological conditions, including wind direction, wind speed, ambient temperature, and RH, were continuously measured from the Mt. Hua meteorological station. All the instruments for aerosol measurements were placed in an air-conditioned room, where temperature was maintained at 25 ℃. The aerosol sampling inlet was located on both sides of the room. The aerosol was sampled via a low-flow $PM_{2.5}$ cyclone inlet, passed through a Nafion dryer, and directed to different instruments through stainless steel or conductive black tubing using an isokinetic flow splitter. The sampling air was dried to RH below 20 % using a Nafion diffusion dryer.

2.4 Analysis of air mass origins

To investigate the origins of air masses reaching our observational site, the Hybrid Single Particle Lagrangian Integrated Trajectory (HYSPLIT) transport and dispersion model (Draxler and Hess, 1998) was employed. In the calculations, 72-hour backwards trajectories were computed for air parcels arriving at the sampling location (2060 m a.s.l) with a temporal resolution of 2 hours. This study employed the cluster analysis method proposed by Draxler et al (Stein et al., 2015), where the clustering criterion was defined such that the spatial variance of each cluster corresponds to the sum of squared distances between individual trajectories and the mean trajectory of that cluster. The total spatial variance (TSV) was calculated as the sum of the spatial variances of all clusters. The final clustering result was obtained by minimizing the increase in TSV. The trajectory frequency distributions for the resulting clusters are provided in Fig. S8.

Deleted: 24

3 Results and discussion

3.1 Overview

Figure 1 illustrates the time series of wind direction, wind speed, RH, ambient temperature, $PM_{2.5}$

concentrations, and black carbon (BC) mass concentrations throughout the entire experimental period. Overall, the average wind speed during the campaign was around 5.0 ± 3.2 m/s, with the prevailing wind directions originating from the west and northwest. The $PM_{2.5}$ mass concentration was generally below 20 $\mu g/m^3$, with an average value of 8.2 ± 6.7 $\mu g/m^3$, aligning with the winter 2020 averages observed at the Mt. Hua site reported by Feng et al. (2023) (Feng et al., 2023). In contrast to the heavily polluted Guanzhong Basin urban areas, the average $PM_{2.5}$ levels were notably higher (e.g., 68.0 ± 42.8 $\mu g/m^3$ in Xi'an; Chen et al., 2021). This discrepancy, which is consistent with previous studies (Dai et al., 2018), indicates a comparatively reduced influence of ground-level anthropogenic emissions at the current site, plausibly attributed to particle deposition or dilution during the transport from lower altitudes to the mountaintop (Feng et al., 2023). From Fig. 1, it is clearly to observe that meteorological conditions substantially changed after November 6, characterized by a decrease in temperature, a slight increase in wind speed, and a shift in the wind direction from west to northwest. Due to the significant temperature drop during this period, domestic heating in this area was initiated. The notable differences in the meteorological conditions as well as anthropogenic emissions during the two distinct periods can result in different atmospheric processes and transport of aerosols. This would in turn lead to variations in the aerosol chemical composition as well as their physicochemical properties, in particular, aerosol hygroscopicity. Detailed analysis of aerosol hygroscopicity and their chemical composition, taking into account of the influence of air mass origins and domestic heating activities, for the two periods will be further analyzed in Sect. 3.3.

Fig. 2 (a–e) shows the temporal evolution of the κ-PDF for different particle sizes, with the black line representing the average κ. The results reveal that the average κ for particles at 30, 60, 100, 150, and 200 nm were 0.20, 0.21, 0.25, 0.27, and 0.30, respectively. Chen et al. (2021) obtained an average κ value of 0.14 ± 0.04 for the water-soluble components of 100 nm particles at the ground-level environment of the Guanzhong Basin during winter based on particle chemical composition measurements. Considering the contribution of water-insoluble components, the overall hygroscopicity would be even lower. We observed that at our observational site, water-soluble inorganic components were the dominant composition in particles (average of 77 % in mass fraction, see Fig. 2e), while the organic components contributed the most (54 % in mass fraction) at the ground-level Guanzhong Basin background site. Though bulk-phase chemical composition may deviate from that of size-resolves ones, this may partially explain the large difference in aerosol hygroscopicity between the two sites at the same region. Particles

Deleted:

Deleted: κ-PDF

sampled at the ground level indicating the distinct sources, secondary processes for atmospheric aerosols in the free troposphere compared to ground-level environments.

The averaged κ-PDF in Fig. 3a reveals that particles of different sizes at the current study were dominated by the MH mode, indicating the aerosols at the site had a mild degree of external mixing of different sources. This characteristic is similar to the results from other high-altitude regions, which could be explained by the slight influence of the advection of aerosols from the PBL (Dingenen et al., 2005; Holmgren et al., 2014; Sjogren et al., 2008). As illustrated in Figure 3a, the contribution of the MH mode becomes more pronounced as particle size increases, which means nucleation and Aitken mode particles (diameter at 30 and 60 nm) tend to contain higher number fraction of LH mode particles (see Table 1). Nucleation and Aitken mode particles are typically from new particle formation (NPF) and subsequent growth or anthropogenic sources injected from the PBL. However, NPF events were rarely observed (only once) at the current site during this study, suggesting anthropogenic emissions within the PBL were the primary sources for these smaller, less hygroscopic particles. This finding on the other hand suggests that the larger particles (e.g., 100-200 nm) at the site, characterized by a higher degree of internal mixing, may stem from different origins and are most likely subject to long-range transport with extensive aging processes. This interpretation is supported in part by Li et al. (2011), who conducted measurements during similar seasons at Mt. Hua and reported that particles in the 100–400 nm range were predominantly composed of secondary inorganic species, such as SO_4^{2-}, NO_3^-, and NH_4^+, which typically have experienced longer aging processes.

Formatted: Highlight

Deleted: (

Deleted: ,

Formatted: Highlight

Formatted: Subscript, Highlight

Formatted: Highlight

Deleted: This on the other hand indicates that accumulation mode particles (e.g., those with diameters at 100-200 nm) at the site, characterized by a higher degree of internal mixing, may stem from a different origin, being most likely long-range transported along with extensive aging processes.

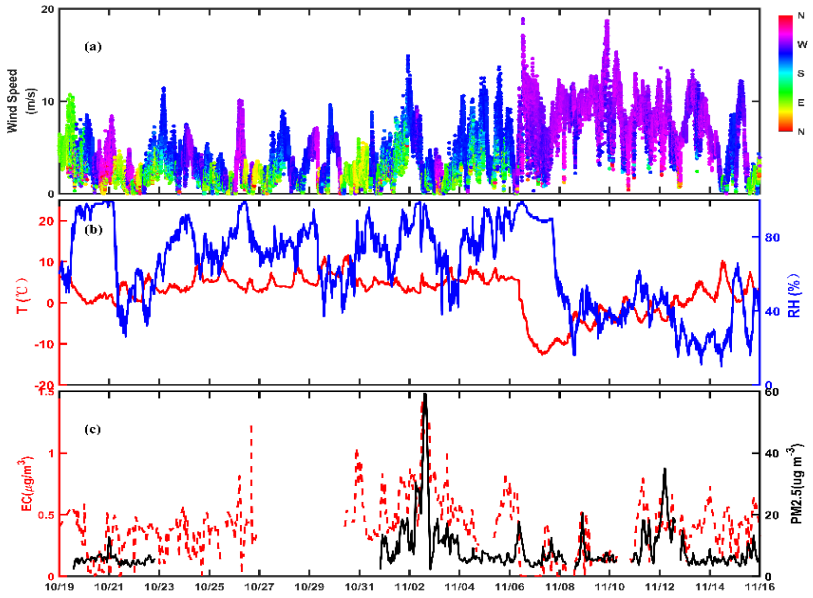

Figure 1. Meteorological conditions over the whole observation period. (a) wind speed, wind direction; (b) the temperature and RH; (c) $PM_{2.5}$ and EC mass concentrations.

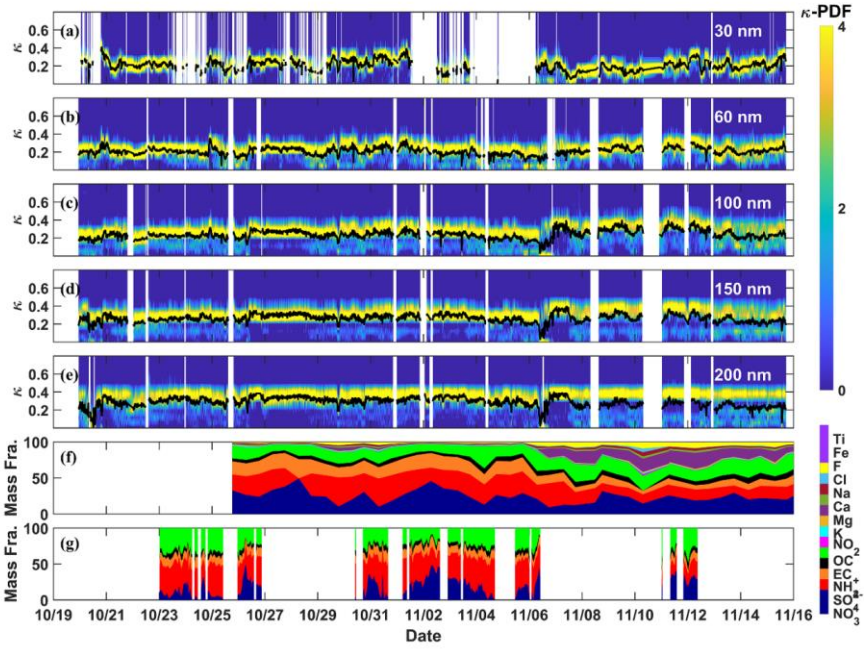

Figure 2. (a-e) Time series of κ-PDF for different particle sizes (with the black line indicating the mean κ value) and (f-g) time series of chemical composition of $PM_{2.5}$ obtained using offline and continuous online measurements, respectively, during the sampling period.

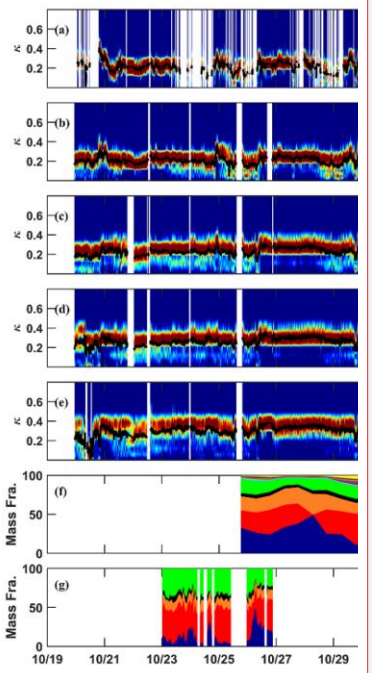

Deleted:

Formatted: Highlight

Formatted: Subscript, Highlight

Formatted: Highlight

Deleted: derived from offline measurements and URG measurement,…

Table 1 Statistics of hygroscopicity parameter κ for particles of different sizes.

Diameter	30 nm	60 nm	100 nm	150 nm	200 nm
All groups					
κ	0.20	0.21	0.25	0.27	0.30
Std. dev	0.06	0.04	0.05	0.04	0.05
More-hygroscopic					
κ	0.27	0.27	0.30	0.32	0.35
Std. dev	0.03	0.02	0.03	0.03	0.03
NF	0.58	0.63	0.74	0.82	0.84
Std. dev	0.28	0.17	0.14	0.12	0.13
Less-hygroscopic					
κ	0.13	0.13	0.11	0.11	0.11
Std. dev	0.04	0.03	0.03	0.03	0.04
NF	0.40	0.35	0.25	0.17	0.16
Std. dev	0.28	0.17	0.13	0.11	0.13

3.2 Diurnal variations of κ-probability density function

Deleted:

Deleted: κ-PDFs

Formatted: Highlight

No clear diurnal variation was observed in the κ-PDF of particles at most sizes at the current site, except for a minor broadening in the κ-PDF during daytime for 30-nm particles, as depicted in Fig. 3b-f. The relatively constant κ-PDF of particles at most sizes throughout the entire day is consistent with the stable diel variation in the number fraction of each hygroscopic mode and their respective hygroscopicity (see Fig. S1). The wider κ-PDF for 30 nm particles during the daytime was mainly attributed to the elevated number fraction of particles in the less-hygroscopic mode. Given that our observational site is consistently located within the residual layer or the free troposphere throughout the day, the influence of vertical diffusion of pollutants from the PBL, being primarily anthropogenic, was expected to be minimal. This is particularly obvious for larger particles, which were abundant at the site, while for smaller particles, this influence became more notable due to their lower concentration that a slight vertical upward transport from the PBL may potentially alter their κ-PDF characteristics.

As aerosol hygroscopicity is ultimately determined by their chemical composition, their diurnal pattern observed aligns neatly with the daily trend in the mass fractions of each component within the particles, as shown in Fig. S2. Note that the chemical composition data from the online measurement were used in this analysis, as the offline measurements, while having better temporal coverage, were limited to half-day resolution. Interestingly, notable differences were observed in meteorological

Deleted: URG

Formatted: Highlight

variables, including ambient temperature and RH, as well as the concentration of atmospheric trace gases like O_3 and SO_2, between daytime and nighttime at the site (see Fig. S3 and Fig. S4). Thus, it is reasonable to expect that, during daytime, under the conditions of higher solar radiation, elevated temperatures, and increased levels of atmospheric oxidants, various secondary species are likely to form, probably through photochemical oxidation processes. These newly-formed species will subsequently partition or condense onto pre-existing particles, thereby altering their chemical composition and, consequently, their hygroscopicity. However, such an influence on aerosol chemical composition and their hygroscopicity was not obviously observed at the current study. A plausible explanation for this could be the insignificant yield of these secondary compounds, potentially due to the scarcity of their atmospheric precursors during this season. These results further confirm that the current aerosols, particularly larger particles, were primarily originated from regional or long-range transport with longer atmospheric aging, with limited contributions from local lower altitude sources or in situ secondary formation.

Deleted: obviously

Formatted: Highlight

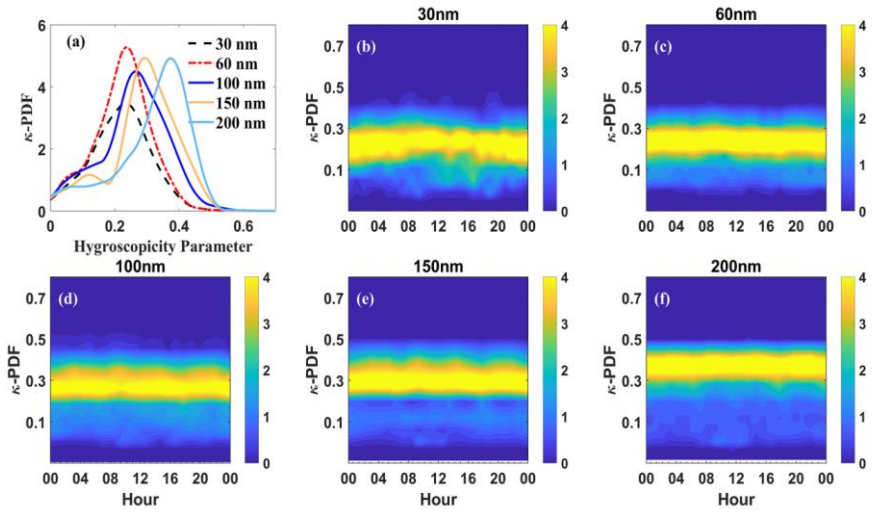

Deleted:

Figure 3. (a) Average κ-PDF for particles at different sizes; (b-f) diurnal variations of the κ-PDF for particles of different sizes measured during the campaign.

3.3 The impact of regional emissions and long-range transport on aerosol hygroscopicity of high-altitude aerosols

Despite the absence of a clear diurnal pattern in the particle chemical composition by online analysis, semi-diurnal offline measurements demonstrated significant compositional changes between the first and second half of the campaign. Specifically, starting from November 6, the contributions of Ca^{2+} and Fe^{2+} to $PM_{2.5}$ mass increased substantially, accounting for up to approximately 20 % of the total particle mass, indicating a shift in aerosol sources after this time. Given that Ca^{2+} and Fe^{2+} are typically recognized as mineral dust tracers (Feng et al., 2023; Kouyoumdjian and Saliba, 2006), these observations strongly suggest an episode of distinct long-range transport of mineral dust after November 6. This signature, being consistent with previous findings (Liu et al., 2024), was further confirmed by the backward trajectory analysis as shown in Fig. 4. The results revealed that air masses arriving at the current site during this time were mainly originated from the northwest, passing through the Mongolia-Inner Mongolia corridor and Tengger Desert region at ~1400 m altitude before reaching our site (Cluster 3 and 5). On the other hand, this period also coincided with the initiation of regional domestic heating, creating a unique scenario where long-range transported dust components mixed with regional emitted anthropogenic pollutants. Consequently, the arriving air masses, enriched with both mineral dust and heating-related emissions, likely modified the background aerosol chemical composition at our observational location (Du et al., 2022).

To comprehensively evaluate the impacts of long-range transport and regional emissions on aerosol hygroscopic properties, we compared the size-resolved aerosol hygroscopicity parameter (κ) across five air mass clusters identified through trajectory analysis (Fig.5a). As Cluster 1, 2 and 4 also occurred during the latter half of the campaign, coinciding with domestic heating activities, we further divided each of these three clusters into two distinct periods. The segments during the domestic heating period of these three clusters were specifically labeled as Cluster 1 DH, Cluster 2 DH and Cluster 4 DH, where "DH" denotes the influence of domestic heating. During the first half of the campaign, which was free from significant influence of mineral dust and prior to the onset of domestic heating activities (i.e., Cluster 1, 2, and 4), aerosols exhibited clear size-dependency of κ, with κ values increasing with increasing particle size. Moreover, the κ values observed for particles of the same sizes were relatively comparable across these three clusters. Air masses associated with these clusters, particularly Cluster 1, mainly

Formatted: Highlight
Formatted: Font: Italic, Highlight
Formatted: Highlight
Formatted: Highlight
Formatted: Font: Italic, Highlight
Formatted: Highlight
Formatted: Font: Italic, Highlight
Formatted: Highlight
Formatted: Font: Italic, Highlight
Formatted: Highlight

transported over relatively short distances from southeastern and southwestern regions, passing through the heavily polluted Guanzhong Plain urban agglomeration and may represent the atmospheric conditions of this regional environment. In contrast, aerosols in Cluster 3, 5 and Cluster 1 DH, 2 DH, and 4 DH displayed relatively constant κ across most particle sizes, except for sub-100nm particles, which probably had local origins rather than long-range transport, as discussed earlier.

For 200 nm particles, Cluster 1, 2, and 4 exhibited the highest κ values (~0.32), followed by Cluster 3 and 5 (~0.27), while the lowest values were observed in Cluster 1 DH, 2 DH, and 4 DH (~0.22). Given that the chemical composition of bulk aerosols is more representative of larger particles than smaller ones (Hong et al., 2018), this pattern was consistent with the average aerosol composition measured by the online measurements. During Cluster 1, 2, and 4, aerosols were dominated by inorganic species, such as NH_4^+, SO_4^{2-}, NO_3^-, which are highly hygroscopic and accounted for over 70 % of the $PM_{2.5}$ mass fraction (see Fig.6).

For Cluster 3 and 5, the contribution of these inorganic species decreased markedly, dropping from over 70 % to less than 50 % in mass fraction, as shown in Fig.6. Concurrently, the levels of Ca^{2+}, Fe^{2+} increased substantially, from less 1 % to approximately 20 % of $PM_{2.5}$ mass. This shift may partially explain both the reduced hygroscopicity ($\kappa \approx 0.09$) and the elevated number fraction (21 %) of LH mode particles in these clusters compared to those ($\kappa \approx 0.12$, NF_{LH} = 10 %) in Cluster 1, 2, and 4, as these mineral dust components are generally hydrophobic or weakly hygroscopic. The influence of mineral dust was further confirmed by the strong correlation between SO_4^{2-} with Ca^{2+} ($R^2 = 0.83$) in Cluster 3 and 5, contrasting with their weak associations ($R^2 \approx 0.1$) during other clusters, where SO_4^{2-} was instead well linked to NH_4^+ ($R^2 \approx 0.9$) (see Fig.7). The co-variation of SO_4^{2-} and Ca^{2+} indicates that they possibly shared the same origins (Sullivan et al., 2009), with Ca^{2+} likely existing in the form of nearly non-hygroscopic $CaSO_4$ ($\kappa \approx 0.01$-0.05) during this episode, reinforcing the observed hygroscopicity decline relative to Cluster 1, 2, and 4. On the other hand, as particle size decreased, a slight increase in the overall aerosol hygroscopicity was observed in Cluster 3 and 5, which can be explained by the enhanced hygroscopicity of LH mode particles coupled with a small decrease in their number fraction. Given that mineral dust mainly resided in larger particles, this size-dependent trend in hygroscopicity suggests a reduced contribution of mineral dust to the hygroscopicity of smaller particles within Cluster 3 and 5.

As noted earlier, beginning on November 6, which encompassed the entire duration of Cluster 3, 5,

Formatted ...

Formatted ...

Deleted: 5

Formatted: Highlight

Deleted: 5

Formatted ...

1 DH, 2 DH, and 4 DH, regional domestic heating was initiated, which may emit substantial amounts of primary aerosols, such as black carbon (BC) and primary organic aerosols (POA). These aerosols were likely transported to our observational site via advection. This interpretation aligns with the findings of Du et al. (2022), who reported a marked increase in the fraction of organic aerosols as well as BC at Mt. Hua following the initiation of domestic heating. Though no direct source apportionment of organic aerosols can be obtained by the current study, a moderate increase (approximately 7 %) in the organic mass fraction in $PM_{2.5}$ during Cluster 3 and 5, followed by a more pronounced rise in both organic (10 %) and BC fractions (5 %) during Cluster 1 DH, 2 DH, and 4 DH was observed compared to other clusters (see Fig.6), further supporting our previous hypothesis. Thus, the elevated levels of these primary aerosols, typically exhibited weak hygroscopicity (Shi et al., 2022), coupled with the high contents of weakly hygroscopic mineral dust, may synergistically drive the continued decline in aerosol hygroscopicity throughout this period.

Despite both being influenced by dust events and domestic heating activities, aerosols in Cluster 5 exhibited higher aerosol hygroscopicity (0.25) compared to Cluster 3 (0.23), mainly due to their larger number fraction of MH mode particles, accompanied by the higher hygroscopicity of LH mode particles, as shown in Fig.5. Interestingly, striking high RH levels (around 80 %) were observed in Cluster 5, which nearly doubled the values in Cluster 3 (see Fig.S5). Such high-RH conditions may facilitate some specific aerosol processes, such as multi-phase or aqueous phase reactions, potentially altering their chemical composition and may explain their elevated hygroscopicity (Tong et al., 2020). This hypothesis aligns with the results of Du et al. (2022), who observed that the contribution of aqueous-formed water soluble oxidized organic aerosols to the total water-soluble organic aerosols increased from 11.21 % under low-RH levels to over 40 % at RH > 80 %, indicating a significant transformation in the organic aerosol composition. On the other hand, we noticed that the average κ of MH mode particles in Cluster 3 and 5 was markedly greater relative to other clusters (see Fig.5). Following our preceding reasoning, we suspected that the multi-phase or aqueous phase reactions under higher-RH levels in Cluster 5, not only enhanced the hygroscopicity of LH mode particles, but also produced substantial highly hygroscopic materials, which may have persisted until the entire duration of Cluster 3 and 5. However, without detailed compositional analysis at molecular level, the exact mechanisms responsible for this exceptionally high aerosol hygroscopicity remained unclear.

In summary, during the first half of the campaign, when air masses mainly passed through the

Formatted: Highlight

Formatted: Subscript, Highlight

Formatted: Highlight

Deleted: 5

Formatted: Highlight

Deleted: 6

Formatted: Highlight

Formatted: Highlight

Formatted: Font: Italic, Highlight

Formatted: Highlight

Deleted: 6

Formatted: Highlight

Deleted: To comprehensively evaluate the influence of long-range transport and regional emissions on aerosol hygroscopic properties, we compared the size-resolved aerosol hygroscopicity parameter κ among six trajectory-identified air mass clusters (Fig.5a). During the periods without significant influence of mineral dust and prior to the heating activities (i.e., Cluster 1, 2, 4 and 6), aerosols particles showed a clear size-dependency of κ, with comparable κ values observed for particles at the same sizes. Air masses associated with these clusters, particularly Cluster 1 and 4, primarily transported over relatively short distances from southeastern and southwestern regions. These trajectories passed through the heavily polluted Guanzhong Basin urban agglomeration, potentially reflecting the atmospheric characteristics of this region. In contrast, aerosol particles in Cluster 3 and 5 displayed relatively constant κ across most particle sizes, except for particles smaller than 100 nm, which probably had local origins rather than long-range transport, as previously discussed.

Formatted: Font colour: Auto

heavily polluted Guanzhong Plain urban agglomeration, aerosols were primarily composed of secondary inorganic species and exhibited the highest hygroscopicity. Starting around November 6, increased influences from both mineral dust and domestic heating activities led to a noticeable decline in aerosol hygroscopicity, particularly in larger particles. This reduction was largely attributed to the rising levels of weakly hygroscopic components, such as mineral dust tracers (e.g., Ca^{2+}, Fe^{2+}), organic components as well as BC, highlighting the combined effects of long-range transport and regional emissions on aerosol composition and properties.

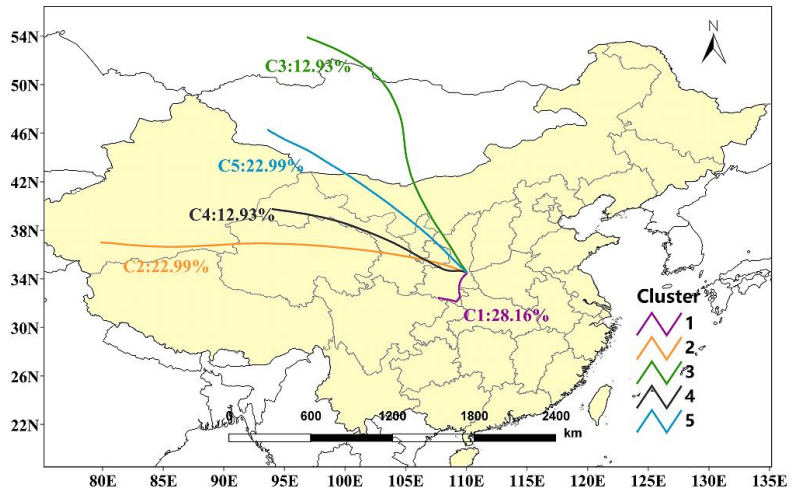

Figure 4. Cluster analysis of 72 h backward trajectories at 2060 m above ground level at the sampling site during the five trajectory-identified clusters. The line colors denote different clusters, i.e., purple for Cluster 1, yellow for Cluster 2, green for Cluster 3, black for Cluster 4, and blue for Cluster 5.

Deleted: In Cluster 5, 200 nm particles showed the lowest κ value (~0.25) compared to other clusters (0.3). This reduction in overall hygroscopicity is attributed to the decreased hygroscopicity ($\kappa \approx 0.08$) and elevated number fraction (23 %) of LH mode particles, in contrast to other clusters where LH particles constituted 15% in numbers with $\kappa \approx$ 0.12. Consistent with expectation, the increased fraction of LH mode particles may partly originate from mineral dust, as they were typically hydrophobic or weakly hygroscopic. This mineral dust influence was further confirmed by the strong correlation between SO_4^{2-} with Ca^{2+} ($R^2 = 0.83$) in Cluster 5, contrasting with their weak associations ($R^2 \approx 0.1$) during other clusters, where SO_4^{2-} instead well linked to NH_4^+ ($R^2 \approx$ 0.78). The co-variation of SO_4^{2-} and Ca^{2+} indicates that they possibly shared the same origins (Sullivan et al., 2009), and Ca^{2+} may primarily exist in the form of hydrophobic $CaSO_4$ ($\kappa \approx$ 0.01-0.05) during this episode, reinforcing the observed hygroscopicity decline. Furthermore, domestic heating activities were a significant source of primary organic aerosol particles, which exhibited weak hygroscopicity as suggested by previous studies (Shi et al., 2022) and may also contribute to the elevated proportion of LH mode particles during this episode. Though no direct source apportionment of organic aerosols can be obtained by the current study, a notably higher fraction of organic aerosols was observed in $PM_{2.5}$ of Cluster 5 compared to other clusters. We hypothesize that the elevated fraction of organic aerosols in Cluster 5 could be primarily driven by domestic heating emissions, consistent with previous study (Du et al., 2020), which reported a substantial rise in the fraction of organic aerosols following the onset of domestic heating. Additionally, Cluster 5 exhibited a slight increase in the overall aerosol hygroscopicity as particle size decreases, which can be explained by the enhanced hygroscopicity of LH mode particles together with a modest reduction in their number fraction. Given that mineral dust mainly resided in large particles (e.g., > 100~200 nm), this observed size-dependent hygroscopicity trend suggests a reduced contribution of mineral dust to the hygroscopicity of smaller particles in Cluster 5.

domestic heating activities, aerosol particles in Cluster 3 exhibited higher hygroscopic growth, mainly due to their larger number fraction of MH mode particles, accompanied ...

Formatted: Font colour: Auto, Highlight

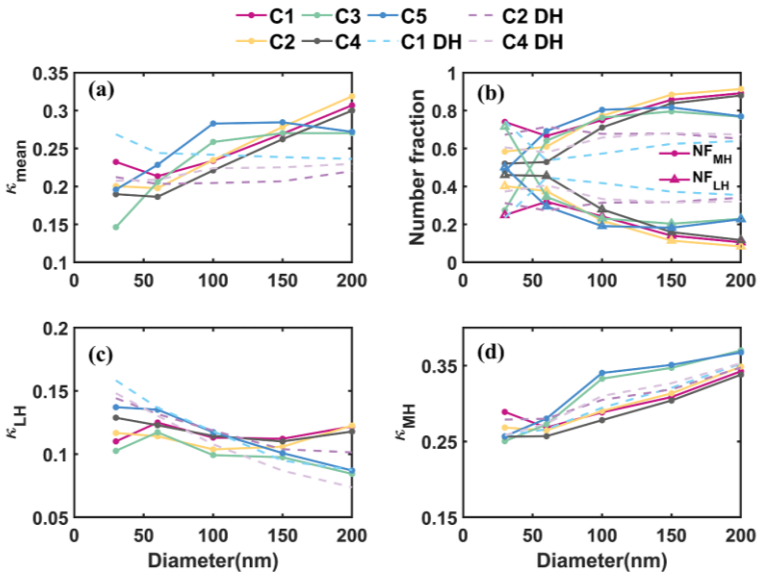

555

Figure 5. Cluster analysis corresponding to (a) mean aerosol hygroscopicity parameters κ, (b) the number fraction of LH and MH mode particles, (c) the mean κ values of LH and MH mode particles at different sizes.

Formatted: Indent: First line: 2 ch, No widow/orphan control

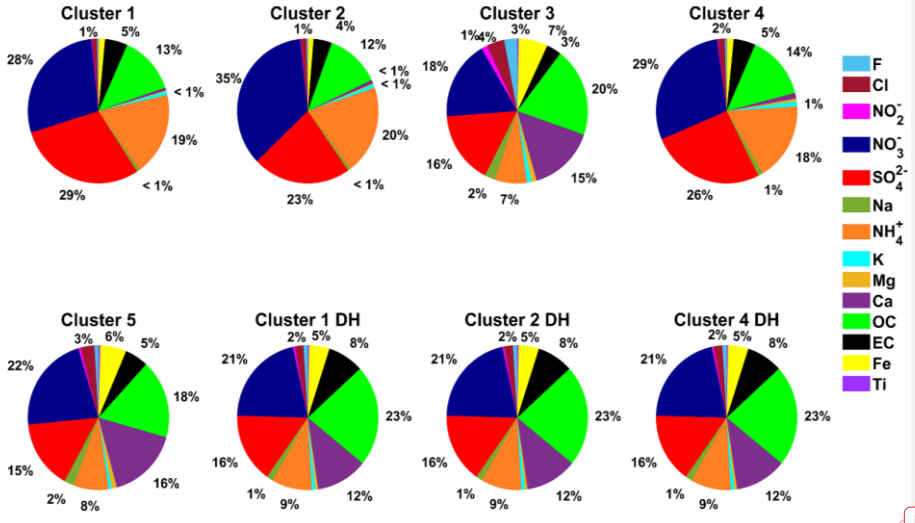

560

Figure 6. Proportions of chemical composition in different clusters.

Formatted: Font: 小五, Font colour: Auto, Highlight

Formatted: Font: 小五, Font colour: Auto, Highlight

Formatted: Font: 小五, Font colour: Auto

Formatted: Justified

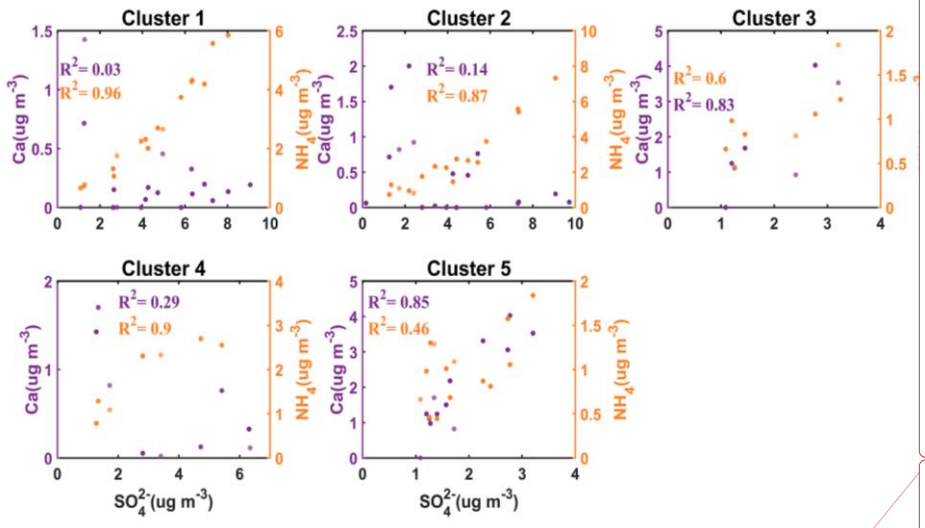

Figure 7. The correlation between $SO4^{2-}$ and Ca^{2+}, and $SO4^{2-}$ and NH_4^+ in $PM_{2.5}$ for different air masses.

3.4 Comparison to other free atmosphere ambient measurements

The unique environment of free tropospheric observation sites, being distant from anthropogenic pollution sources, provides a more representative characterization of regional-scale aerosol properties. However, current measurements of aerosol hygroscopicity in the global free troposphere are remarkably sparse (Fig. 8). These available datasets shows that hygroscopic parameter κ for free tropospheric aerosols typically ranged from 0.15 to 0.35, with ours falling within the median of reported values. Winter-time aerosols at Jungfraujoch (3580 m) revealed comparable hygroscopicity to our results, while their higher annual mean ($\kappa \approx 0.3$) implies substantial contribution from secondary inorganic components or more aged components during other seasons (Kammermann et al., 2010). The Monte Cimone Observatory (Italy), situated in the transition zone between the boundary layer and free troposphere, exhibited slightly reduced aerosol hygroscopicity, likely due to vertical transport of less hygroscopic pollutants, which were less-aged, from the boundary layer (Dingenen et al., 2005). Similarly, at lower-altitude sites, such as Huangshan (1865 m) and Puy de Dôme (1465 m), aerosol hygroscopicity was further reduced as a result of enhanced anthropogenic influence (Asmi et al., 2012; Wu et al., 2018a). These results highlight an altitude gradient in aerosol characteristics, where the influence of boundary

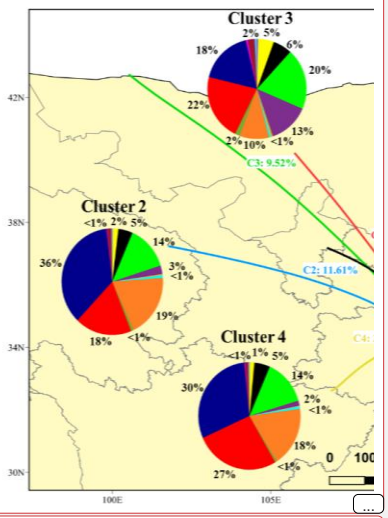

Deleted:

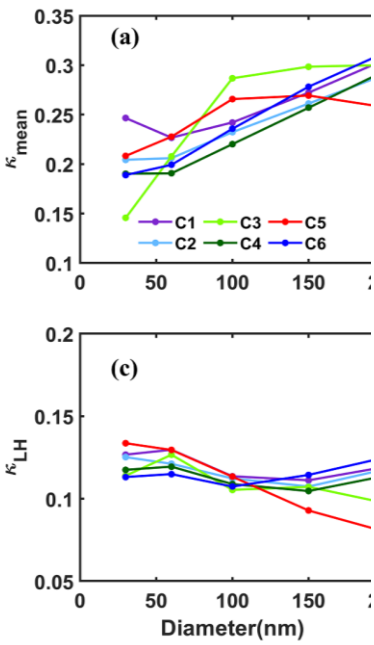

Deleted:

Deleted: 6

Formatted: Font: 小五, Highlight

Formatted: Font: 小五

Deleted: 7

Formatted: Highlight

layer decreased with elevation, resulting in progressively more aged and more hygroscopic aerosols at higher altitudes compared to fresher, less aged and less hygroscopic ones close to the surface. The Izaña Atmospheric Observatory, located in the northeastern Atlantic at 2370 m altitude, provided a different case of marine-influenced aerosol properties (Swietlicki et al., 2000). Their measurements revealed exceptionally high hygroscopicity for 50 nm particles ($\kappa \approx 0.36$), mostly likely stemming from the dominance of inorganic sea salts in the studied particles, contrasting markedly with continental aerosols from tropospheric sites. These comparative analyses demonstrate fundamental differences in atmospheric processes and interactions between free tropospheric and boundary layer environments by distinguishing natural background aerosol properties from anthropogenic influences, these works may establish critical benchmarks for modeling aerosol-climate interactions.

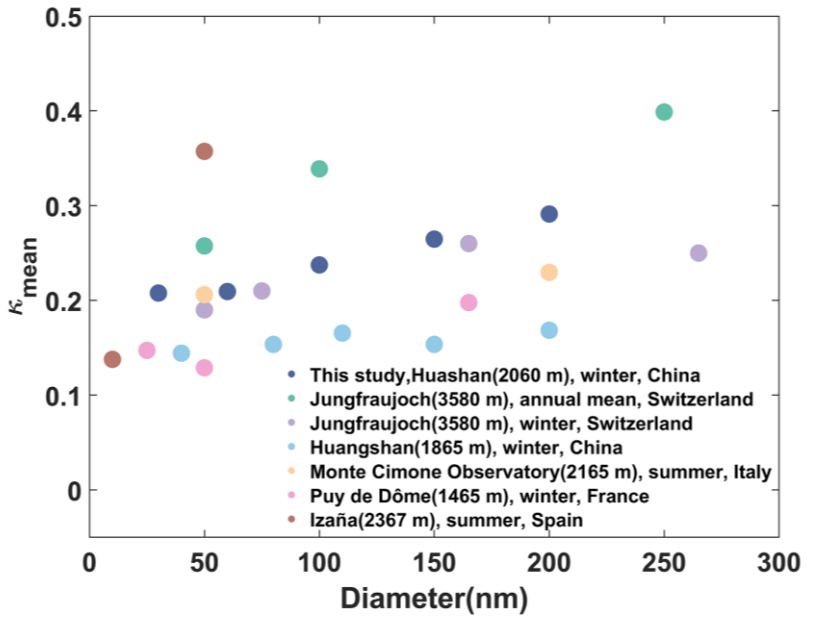

Figure 8. Comparison of aerosol hygroscopicity measured at different high-altitude sites around the world.

Deleted:

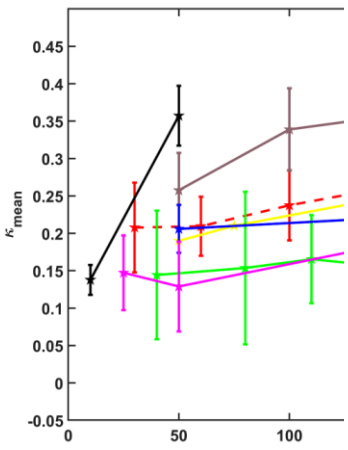

Deleted: 7

Formatted: Highlight

4. Conclusion and implications

This study advances our understanding of aerosol hygroscopicity and mixing states in the lower free troposphere over central China through comprehensive measurements at Mt. Hua (~2060 m a.s.l.). The observed size-dependent hygroscopic growth pattern and externally mixed state of aerosols provide direct evidence of particle transformation during transport in the free troposphere. The absence of diurnal variations in aerosol hygroscopicity confirms minimal influences from boundary layer dynamics, making this site ideal for representing background atmospheric conditions. Particularly noteworthy is the RH-driven hygroscopic enhancement of mineral dust particles, suggesting substantial chemical processes previously underestimated in such environments. These distinct aerosol characteristics highlight the unique atmospheric processes occurring where anthropogenic, natural, and transported air masses interact.

The implications extend beyond investigating long-range transport and free troposphere-boundary layer interactions. Alpine aerosols like those at Mt. Hua act as critical indicators of regional atmospheric properties. Our comparative analysis of mass extinction efficiency (MEE) - a key parameter describing aerosol light attenuation per unit mass, revealed striking altitude dependence: free tropospheric aerosols at the summit exhibited MEE values of 4.29 m^2 g^{-1}, which was three times greater than surface-level observations (1.30 m^2 g^{-1}), despite much lower particle mass aloft. The discrepancy mainly arises from enhanced hygroscopic growth of aged free tropospheric aerosols, which have experienced longer atmospheric processing with reduced influences from local emissions. Such pronounced vertical variations in MEE highlight the necessity of incorporating regional-scale or altitude-resolved hygroscopicity into climate models, particularly for humid or high-altitude settings where such effects may dominate aerosol radiative forcing.

Data availability.

The data of this paper can be obtained from https://doi.org/10.5281/zenodo.15589884 (Shi et al., 2025).

Author contributions.

JH, NM, QW, and LL conceptualized and supervised this study. JS, ZZ, LL YZ, SH, SZ, ML, LX, WR, and JT conducted the field campaign. JS and LL conducted the data analysis. HX contributed to the instrument maintenance. JH, JS, LL, ZZ, NM, JT, YZ, QW discussed the results. JS drew the plots and JH and JS wrote the draft. JH, JS and AW proofed the paper and edited the paper with contributions from all co-authors.

Competing interests.

The authors declare that none of the authors has any competing interests.

Acknowledgments.

This research was supported by the Guangdong Basic and Applied Basic Research Foundation (Grant 2024A1515510020); the "Western Light"-Key Laboratory Cooperative Research Cross-Team Project of Chinese Academy of Sciences (xbzg-zdsys-202219); the Science and Technology Program of Guangdong (2024B1212080002); the National Natural Science Foundation of China (grant no.42175117, 42375072); the Guangzhou basic and applied basic research project-Guangzhou Science and Information Bureau project (grant no. 2025A04J3520), National Natural Science Foundation of China (grant no.32573116).

Formatted: Highlight

Deleted: .

References

Asmi, E., Freney, E., Hervo, M., Picard, D., Rose, C., Colomb, A. and Sellegri, K.: Aerosol cloud activation in summer and winter at puy-de-Dôme high altitude site in France, Atmos. Chem. Phys., 12(23), 11589–11607, doi:10.5194/acp-12-11589-2012, 2012.

Bae, M. S., Schauer, J. J., DeMinter, J. T., Turner, J. R., Smith, D. and Cary, R. A.: Validation of a semi-continuous instrument for elemental carbon and organic carbon using a thermal-optical method, Atmos. Environ., 38(18), 2885–2893, doi:10.1016/j.atmosenv.2004.02.027, 2004.

Bai, Z., Ji, Y., Pi, Y., Yang, K., Wang, L., Zhang, Y., Zhai, Y., Yan, Z. and Han, X.: Hygroscopic analysis of individual Beijing haze aerosol particles by environmental scanning electron microscopy, Atmos. Environ., 172(September 2017), 149–156, doi:10.1016/j.atmosenv.2017.10.031, 2018.

Cai, M., Tan, H., Chan, C. K., Mochida, M., Hatakeyama, S., Kondo, Y., Schurman, M. I., Xu, H., Li, F., Shimada, K., Li, L., Deng, Y., Yai, H., Matsuki, A., Qin, Y. and Zhao, J.: Comparison of aerosol hygroscopcity, volatility, and chemical composition between a suburban site in the Pearl River Delta region and a marine site in Okinawa, Aerosol Air Qual. Res., 17(12), 3194–3208, doi:10.4209/aaqr.2017.01.0020, 2017.

Chen, Y., Wang, X., Peng, H., Li, J., Wang, Y., Wang, G., Li, J., Wu, C. and Liu, L.: Hygroscopicity of Water-Soluble PM2.5 in Rural Northwest China: Contrasting Contributors Between Summer and Winter, J. Geophys. Res. Atmos., 126(15), 1–20, doi:10.1029/2021JD034977, 2021.

Cheng, Y. F., Wiedensohler, A., Eichler, H., Heintzenberg, J., Tesche, M., Ansmann, A., Wendisch, M., Su, H., Althausen, D., Herrmann, H., Gnauk, T., Brüggemann, E., Hu, M. and Zhang, Y. H.: Relative humidity dependence of aerosol optical properties and direct radiative forcing in the surface boundary layer at Xinken in Pearl River Delta of China: An observation based numerical study, Atmos. Environ., 42(25), 6373–6397, doi:10.1016/j.atmosenv.2008.04.009, 2008.

Colbeck, I., Nyeki, S., Li, F., Weingartner, E., Streit, N., G, H. W. and Baltensperger, U.: The background aerosol size distribution in the free troposphere : An analysis of the annual cycle at a high-alpine site, J. Geophys. Res., 103, 31749-31761, doi:10.1029/1998JD200029, 1998.

Dai, Q., Bi, X., Liu, B., Li, L., Ding, J., Song, W., Bi, S., Schulze, B. C., Song, C., Wu, J., Zhang, Y., Feng, Y. and Hopke, P. K.: Chemical nature of $PM_{2.5}$ and PM_{10} in Xi' an , China : Insights into primary emissions and secondary particle formation *, Environ. Pollut., 240, 155–166, doi:10.1016/j.envpol.2018.04.111, 2018.

Dingenen, R. Van, Putaud, J., Santos, S. M. and Raes, F.: Physical aerosol properties and their relation to air mass origin at Monte Cimone (Italy) during the first MINATROC campaign, Atmos. Chem. Phys., 5(2001), 2203–2226, 2005.

Draxler, R. R. and Hess, G. D.: An overview of the HYSPLIT_4 modelling system for trajectories, dispersion and deposition, Aust. Meteorol. Mag., 47(4), 295–308, 1998.

Du, A., Li, Y., Sun, J., Zhang, Z., You, B., Li, Z., Chen, C. and Li, J.: Rapid transition of aerosol optical properties and water-soluble organic aerosols in cold season in Fenwei Plain, Sci. Total Environ., 829, 154661, doi:10.1016/j.scitotenv.2022.154661, 2022.

Farkas, Á., Füri, P., Thén, W. and Salma, I.: Effects of hygroscopic growth of ambient urban aerosol particles on their modelled regional and local deposition in healthy and COPD-compromised human respiratory system, Sci. Total Environ., 806, 151202, doi:10.1016/j.scitotenv.2021.151202, 2022.

Feng, Q., Liu, H., Dai, W., Cao, Y., Shen, M., Liu, Y., Qi, W., Chen, Y., Guo, X., Zhang, Y., Li, L., Zhou, B. and Li, J.: Comparison of chemical composition and acidity of size-resolved inorganic aerosols at the top and foot of Mt. Hua, Northwest China: The role of the gas-particle distribution of ammonia, Sci. Total Environ., 905(May), doi:10.1016/j.scitotenv.2023.166985, 2023.

Gysel, M., McFiggans, G. B. and Coe, H.: Inversion of tandem differential mobility analyser (TDMA) measurements, J. Aerosol Sci., 40(2), 134–151, doi:10.1016/j.jaerosci.2008.07.013, 2009.

Han, S., Hong, J., Luo, Q., Xu, H., Tan, H., Wang, Q., Tao, J., Zhou, Y., Peng, L., He, Y., Shi, J., Ma, N., Cheng, Y. and Su, H.: Hygroscopicity of organic compounds as a function of organic functionality, water solubility, molecular weight, and oxidation level, Atmos. Chem. Phys., 22(6), 3985–4004, doi:10.5194/acp-22-3985-2022, 2022.

Holmgren, H., Sellegri, K., Hervo, M., Rose, C., Freney, E., Villani, P. and Laj, P.: Hygroscopic properties and mixing state of aerosol measured at the high-altitude site Puy de Dôme (1465 m a.s.l.), France, , (14), 9537–9554, doi:10.5194/acp-14-9537-2014, 2014.

Hong, J., Xu, H., Tan, H., Yin, C., Hao, L., Li, F., Cai, M., Deng, X., Wang, N., Su, H., Cheng, Y., Wang, L., Petäjä, T. and Kerminen, V. M.: Mixing state and particle hygroscopicity of organic-dominated aerosols over the Pearl River Delta region in China, Atmos. Chem. Phys., 18(19), 14079–14094, doi:10.5194/acp-18-14079-2018, 2018.

Kammermann, L., Gysel, M., Weingartner, E. and Baltensperger, U.: 13-month climatology of the aerosol hygroscopicity at the free tropospheric site Jungfraujoch (3580ma.s.l.) L., , (10), 10717–10732,

doi:10.5194/acp-10-10717-2010, 2010.

Kouyoumdjian, H. and Saliba, N. A.: Mass concentration and ion composition of coarse and fine particles in an urban area in Beirut : effect of calcium carbonate on the absorption of nitric and sulfuric acids and the depletion of chloride, Atmos. Chem. Phys., (6), 1865–1877, 2006.

Li, J., Wang, G., Zhou, B., Cheng, C., Cao, J., Shen, Z. and An, Z.: Chemical composition and size distribution of wintertime aerosols in the atmosphere of Mt . Hua in central China, Atmos. Environ., 45(6), 1251–1258, doi:10.1016/j.atmosenv.2010.12.009, 2011.

Liu, H., Feng, Q., Huang, Y., Wu, F., Liu, Y., Shen, M., Guo, X. and Li, J.: Composition and size distribution of wintertime inorganic aerosols at ground and alpine regions of northwest China, , 35, doi:10.1016/j.cclet.2024.109636, 2024.

Liu, P. F., Zhao, C. S., Göbel, T., Hallbauer, E., Nowak, A., Ran, L., Xu, W. Y., Deng, Z. Z., Ma, N., Mildenberger, K., Henning, S., Stratmann, F. and Wiedensohler, A.: Hygroscopic properties of aerosol particles at high relative humidity and their diurnal variations in the north China plain, Atmos. Chem. Phys., 11(7), 3479–3494, doi:10.5194/acp-11-3479-2011, 2011.

Liu, X., Gu, J., Li, Y., Cheng, Y., Qu, Y., Han, T., Wang, J., Tian, H., Chen, J. and Zhang, Y.: Increase of aerosol scattering by hygroscopic growth: Observation, modeling, and implications on visibility, Atmos. Res., 132–133, 91–101, doi:10.1016/j.atmosres.2013.04.007, 2013.

Petters, M. D. and Kreidenweis, S. M.: A single parameter representation of hygroscopic growth and cloud condensation nucleus activity, Atmos. Chem. Phys., 7, 1961–1971, doi:10.5194/acp-7-1961-2007, 2007.

Rosenfeld, D., Steven Sherwood, Wood, R. and Donner, L.: Climate Effects of Aerosol-Cloud Interactions, Science (80-.)., 343(January), 379–380, doi:10.1126/science.1247490, 2014.

Shen, M., Qi, W., Guo, X., Dai, W., Wang, Q., Liu, Y., Zhang, Y., Cao, Y., Chen, Y., Li, L., Liu, H., Cao, J. and Li, J.: Influence of vertical transport on chemical evolution of dicarboxylic acids and related secondary organic aerosol from surface emission to the top of Mount Hua, Northwest China, Sci. Total Environ., 858(October 2022), 159892, doi:10.1016/j.scitotenv.2022.159892, 2023.

Shi, J., Hong, J., Ma, N., Luo, Q., He, Y., Xu, H. and Tan, H.: Measurement report : On the difference in aerosol hygroscopicity between high and low relative humidity conditions in the North China Plain, Atmos. Chem. Phys., (22), 4599–4613, 2022, doi:10.5194/acp-22-4599-2022.

Sjogren, S., Gysel, M., Weingartner, E., Alfarra, M. R., Duplissy, J., Cozic, J., Crosier, J. and Coe, H.:

Hygroscopicity of the submicrometer aerosol at the high-alpine site Jungfraujoch , 3580 m a.s.l., Switzerland, , 5715–5729, doi:10.5194/acp-22-4599-2022, 2008.

Stein, Draxler, Rolph, Stunder and Cohen: Noaa's hysplit atmospheric transport and dispersion modeling system, Bull. Am. Meteorol. Soc., (December), 2059–2078, doi:10.1175/BAMS-D-14-00110.1, 2015.

Su, H., Rose, D., Cheng, Y. F., Gunthe, S. S., Massling, A., Stock, M., Wiedensohler, A., Andreae, M. O. and Poschl, U.: Hygroscopicity distribution concept for measurement data analysis and modeling of aerosol particle mixing state with regard to hygroscopic growth and CCN activation, Atmos. Chem. Phys., 10(15), 7489–7503, doi:10.5194/acp-10-7489-2010, 2010.

Swietlicki, E., Zhou, J., Covert, D. S., Hameri, K., Busch, B., Vakeva, M., Dusek, U., Berg, O. H., Wiedensohler, A., Aalto, P., Makela., Martinsson, B. G., Papaspiropoulos, G., Mentes, B., Frank, G. and and Stratmann, F.: Hygroscopic properties of aerosol particles in the northeastern Atlantic during ACE-2, Tellus, (52B), 201–227, 2000.

Swietlicki, E., Hansson, H. C., Hämeri, K., Svenningsson, B., Massling, A., Mcfiggans, G., Mcmurry, P. H., Petäjä, T., Tunved, P., Gysel, M., Topping, D., Weingartner, E., Baltensperger, U., Rissler, J., Wiedensohler, A. and Kulmala, M.: Hygroscopic properties of submicrometer atmospheric aerosol particles measured with H-TDMA instruments in various environments - A review, Tellus, Ser. B Chem. Phys. Meteorol., 60 B(3), 432–469, doi:10.1111/j.1600-0889.2008.00350.x, 2008.

Tan, H., Xu, H., Wan, Q., Li, F., Deng, X., Chan, P. W., Xia, D. and Yin, Y.: Design and application of an unattended multifunctional H-TDMA system, J. Atmos. Ocean. Technol., 30(6), 1136–1148, doi:10.1175/JTECH-D-12-00129.1, 2013.

Tong, Y., Pospisilova, V., Qi, L., Duan, J., Gu, Y., Kumar, V., Rai, P., Stefenelli, G., Wang, L., Wang, Y., Zhong, H., Baltensperger, U., Cao, J., Huang, R., Prevot, A. S. H. and Slowik, J. G.: Quantification of solid fuel combustion and aqueous chemistry contributions to secondary organic aerosol during wintertime haze events in Beijing, Atmos. Chem. Phys. Discuss., (August), 1–41, doi:10.5194/acp-2020-835, 2020.

Wang, G., Kawamura, K., Cheng, C., Li, J., Cao, J., Zhang, R., Zhang, T., Liu, S., Zhao, Z. and Summer, N.: Molecular distribution and stable carbon isotopic composition of dicarboxylic acids, ketocarboxylic acids, and α -dicarbonyls in size-resolved atmospheric particles from Xi' an city, China, Environ. Sci. Technol., (46), 4783−4791, doi:10.1021/es204322c, 2012.

Wang, Y., Chen, Y., Wu, Z., Shang, D., Bian, Y., Du, Z., H. Schmitt, S., Su, R., I. Gkatzelis, G., Schlag,

Formatted: Highlight

Deleted: Molecular Distribution and Stable Carbon Isotopic Composition of Dicarboxylic Acids , Ketocarboxylic Acids , and α -Dicarbonyls in Size-Resolved Atmospheric Particles From Xi ' an City , China,

P., Hohaus, T., Voliotis, A., Lu, K., Zeng, L., Zhao, C., Rami Alfarra, M., McFiggans, G., Wiedensohler, A., Kiendler-Scharr, A., Zhang, Y. and Hu, M.: Mutual promotion between aerosol particle liquid water and particulate nitrate enhancement leads to severe nitrate-dominated particulate matter pollution and low visibility, Atmos. Chem. Phys., 20(4), 2161–2175, doi:10.5194/acp-20-2161-2020, 2020.

Wu, Y., Qiu, Y., Guo, J., Wang, K., Wang, J. and Xuedong, Z.: An Observational study on the hygroscopic properties of aerosol particles at different altitudes - a case study in the Mt. Huangshan, Resour. Environ. Yangtze Basin, (27), 1361–1370, 2018a.

Wu, Z., Wang, Y., Tan, T., Zhu, Y., Li, M., Shang, D., Wang, H., Lu, K., Guo, S., Zeng, L. and Zhang, Y.: Aerosol liquid water driven by anthropogenic inorganic salts: implying its key role in haze formation over the North China Plain, Environ. Sci. Technol. Lett., 5(3), 160–166, doi:10.1021/acs.estlett.8b00021, 2018b.

Deleted: Study

Formatted: Highlight

Deleted: Hygroscopic

Deleted: Properties

Deleted: Aerosol

Deleted: Particles

Deleted: Different

Deleted: Altitudes

Deleted: A

Deleted: Case

Deleted: Study

Formatted: Highlight

Deleted: Aerosol Liquid Water Driven by Anthropogenic Inorganic Salts: Implying Its Key Role in Haze Formation over the North China Plain,